Structural Engineering and Mechanics, *Vol. 62, No. 1 (2017) 33-42*
DOI: https://doi.org/10.12989/sem.2017.62.1.033

Nonlinear torsional analysis of 3D composite beams using the extended St. Venant solution

Kyungho Yoon[1a], Do-Nyun Kim[1,2b] and Phill-Seung Lee[*3]

[1]*Department of Mechanical and Aerospace Engineering, Seoul National University, Gwanak-ro 1, Gwanak-gu, Seoul 08826, Republic of Korea*
[2]*Institue of Advanced Machines and Design, Seoul National University, Gwanak-ro 1, Gwanak-gu, Seoul 08826, Republic of Korea*
[3]*Department of Mechanical Engineering, Korean Advanced Institute for Science and Technology, 291 Daehak-ro, Yuseong-gu, Daejeon 34141, Republic of Korea*

(Received April 15, 2016, Revised August 22, 2016, Accepted December 9, 2016)

Abstract. We present in this paper a finite element formulation for nonlinear torsional analysis of 3D beams with arbitrary composite cross-sections. Since the proposed formulation employs a continuum mechanics based beam element with kinematics enriched by the extended St. Venant solutions, it can precisely account higher order warping effect and its 3D couplings. We propose a numerical procedure to calculate the extended St. Venant equation and the twisting center of an arbitrary composite cross-section simultaneously. The accuracy and efficiency of the proposed formulation are thoroughly investigated through representative numerical examples.

Keywords: nonlinear analysis; finite element method; beam; composite; torsion; warping

1. Introduction

Composite beams are widely used in many engineering applications including aircraft wings, helicopter rotor blades, robot arms and bridges (Librescu 2006, Hodges 2006, Tasi 1992). One of the advantages of using composite beams is that their overall stiffness and strength can be precisely controlled to satisfy the design requirements. However, composite beams may exhibit complex nonlinear mechanical behaviors because the deformation modes such as stretching, bending, shearing, and twisting are usually highly coupled to one another, rendering their analysis and design difficult.

In particular, the warping effect must be accurately modeled in finite element analysis of beams in order to obtain a reliable solution for their torsional behaviors (Bathe 2014, Timoshenko and Goodier 1970, Vlasov, 1961, Yoon and Lee 2014, Ishaquddin *et al*. 2012, Rand 1998, Lee and Lee 2004). This becomes even more important for the analysis of composite beams because significant coupling exists between the deformation modes, and hence, inaccurate consideration of the warping effect may deteriorate the solution accuracy of the beam element not only under torsion but also under other loading types.

A considerable amount of research effort on developing accurate and efficient warping models for composite beams has been made in mathematical theories and their finite element implementations (Giavotto *et al*. 1983, Horgan and Simmonds 1994, Yu *et al*. 2002, Yu *et al*. 2005, Cortinez and Piovan 2006, Cardoso *et al*. 2009, Sapountzakis and Tsipiras 2010, Høgsberg and Krenk 2014). Most recent theoretical approaches focus on the secondary warping effect (Fatmi and Ghazouani 2011, Genoese *et al*. 2014, Tsipiras and Sapointzakis 2012) and Wagner effect (Popescu and Hodges 1999, Pi *et al*. 2005, Mohri *et al*. 2008) which may lead to mechanical behaviors of composite beams significantly different from those predicted by classical theories. Nevertheless, most beam elements developed so far cannot fully represent the complex, highly coupled 3D behaviors of composite beams. Furthermore, their nonlinear behaviors in geometry and material properties have rarely been explored.

The objective of this paper is to present the finite element formulation for geometric and/or material nonlinear analysis of beams with arbitrary composite cross-sections. The remarkable accuracy and efficiency of the proposed beam element are attributed to the employment of the continuum mechanics based beam formulation that naturally accounts for variations in geometry and material properties within the cross-section as well as along the beam axis. In particular, the warping function and the corresponding twisting center are calculated simultaneously for any composite beam based on the extended St. Venant equations within our framework. As a result, the proposed element can predict complex and non-intuitive three-dimensional behaviors of composite beams under any type of loading and boundary conditions. The formulation is simple and straightforward for both geometric and material nonlinear analyses as it is based on well-established continuum mechanics.

In the following sections, we briefly review the nonlinear formulation of the continuum mechanics based beam element, present our method to calculate the warping

*Corresponding author, Associate Professor
E-mail: phillseung@kaist.edu
[a]Postdoctoral Researcher
[b]Associate Professor

http://www.techno-press.org/?journal=sem&subpage=8
ISSN: 1225-4568 (Print), 1598-6217 (Online)

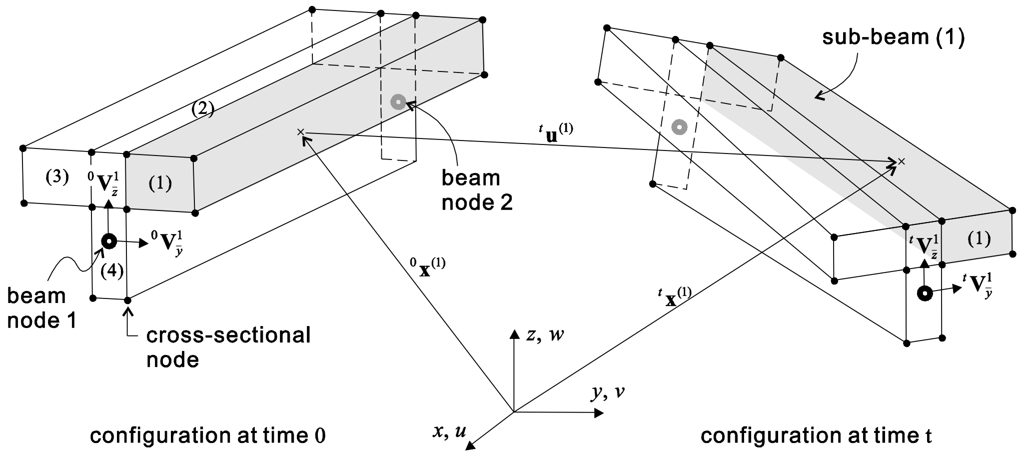

Fig. 1 A 2-node continuum mechanics based beam element with 4 sub-beams in the configurations at time 0 and *t*

function for an arbitrary composite cross-section and demonstrate the usefulness of the proposed beam element via several numerical examples. Finally, we conclude with a summary and possible future directions of the current research.

2. Continuum mechanics based beam elements

In this section, we review the nonlinear formulation of the continuum mechanics based beam finite elements (Yoon and Lee 2014, Yoon *et al*. 2012). Within the total Lagrangian framework, the proposed nonlinear formulation adopted in this study can describe large twisting kinematics accurately coupled with stretching, bending, shearing and warping.

Fig. 1 represents a 2-node continuum mechanics based beam consisting of 4 sub-beams in the configurations at time 0 and *t*, in which basic variables used for the beam element are schematically defined. In the *q*-node continuum mechanics based beam, the geometry interpolation for sub-beam *m* is described using

$$
\begin{aligned}
{}^t\mathbf{x}^{(m)} &= \sum_{k=1}^{q} h_k(r)\,{}^t\mathbf{x}_k + \sum_{k=1}^{q} h_k(r)\bar{y}_k^{(m)}\,{}^t\mathbf{V}_{\bar{y}}^k \\
&+ \sum_{k=1}^{q} h_k(r)\bar{z}_k^{(m)}\,{}^t\mathbf{V}_{\bar{z}}^k + \sum_{k=1}^{q} h_k(r) f_k^{(m)}\,{}^t\alpha_k\,{}^t\mathbf{V}_{\bar{x}}^k
\end{aligned}
\tag{1}
$$

$$
\begin{aligned}
\text{with}\quad \bar{y}_k^{(m)} &= \sum_{j=1}^{p} h_j(s,t)\bar{y}_k^{j(m)}\ ,\quad \bar{z}_k^{(m)} = \sum_{j=1}^{p} h_j(s,t)\bar{z}_k^{j(m)}\ , \\
f_k^{(m)} &= \sum_{j=1}^{p} h_j(s,t) f_k^{j(m)}
\end{aligned}
\tag{2}
$$

where ${}^t\mathbf{x}^{(m)}$ is the material position vector at time *t*, $h_k(r)$ is the 1D shape function at beam node *k* (C_k), ${}^t\mathbf{x}_k$ is the position vector of beam node *k* at time *t*, ${}^t\mathbf{V}_{\bar{x}}^k$, ${}^t\mathbf{V}_{\bar{y}}^k$ and ${}^t\mathbf{V}_{\bar{z}}^k$ are the director vectors at time *t* orthonormal to each other, and ${}^t\alpha_k$ is the corresponding warping degree of freedom at beam node *k* at time *t*. In Eq. (2), $h_j(s,t)$ represents the 2D shape function at cross-sectional node *j*, $\bar{y}_k^{j(m)}$ and $\bar{z}_k^{j(m)}$ are the coordinates of cross-sectional node *j*, and $f_k^{j(m)}$ is the value of warping function at cross-sectional node *j*. The calculation methodology of warping function for arbitrary composite cross-sections is presented in Section 3.

The covariant components of the Green-Lagrange strain tensor in the configuration at time *t*, referred to the configuration at time 0, are defined as

$$
\begin{aligned}
{}_0^t\varepsilon_{ij}^{(m)} &= \frac{1}{2}\left({}^t\mathbf{g}_i^{(m)}\cdot{}^t\mathbf{g}_j^{(m)} - {}^0\mathbf{g}_i^{(m)}\cdot{}^0\mathbf{g}_j^{(m)}\right) \\
\text{with}\quad {}^t\mathbf{g}_i^{(m)} &= \frac{\partial\,{}^t\mathbf{x}^{(m)}}{\partial r_i}
\end{aligned}
\tag{3}
$$

where ${}_0^t\varepsilon_{22}^{(m)}$, ${}_0^t\varepsilon_{33}^{(m)}$, and ${}_0^t\varepsilon_{23}^{(m)}$ are zero according to the assumption of Timoshenko beam theory. The covariant strain components are used to construct an assumed strain field of the element in order to circumvent shear and membrane locking problems, which is achieved in this study using the MITC (Mixed Interpolation of Tensorial Components) scheme (Yoon and Lee 2014, Lee and McClure 2006).

The local strain components are calculated as

$$
\begin{aligned}
{}_0^t\bar{\boldsymbol{\varepsilon}}^{(m)} &= \left[{}_0^t\bar{\varepsilon}_{11}^{(m)}\quad 2\,{}_0^t\bar{\varepsilon}_{12}^{(m)}\quad 2\,{}_0^t\bar{\varepsilon}_{13}^{(m)}\right]^T \\
\text{with}\quad ({}^0\mathbf{t}_i\otimes{}^0\mathbf{t}_j)\,{}_0^t\bar{\varepsilon}_{ij}^{(m)} &= ({}^0\mathbf{g}^{k(m)}\otimes{}^0\mathbf{g}^{l(m)})\,{}_0^t\varepsilon_{kl}^{(m)}
\end{aligned}
\tag{4}
$$

where the base vectors for the local Cartesian coordinate system are obtained by interpolating the nodal director vectors

$$
\begin{aligned}
{}^0\mathbf{t}_1 = h_k(r)\,{}^0\mathbf{V}_{\bar{x}}^k\ ,\quad {}^0\mathbf{t}_2 &= h_k(r)\,{}^0\mathbf{V}_{\bar{y}}^k \\
\text{and}\quad {}^0\mathbf{t}_3 &= h_k(r)\,{}^0\mathbf{V}_{\bar{z}}^k
\end{aligned}
\tag{5}
$$

The corresponding second Piola-Kirchhoff stresses are defined as

$$
{}_0^t\bar{\mathbf{S}}^{(m)} = \bar{\mathbf{C}}^{(m)}\,{}_0^t\bar{\boldsymbol{\varepsilon}}^{(m)}
$$

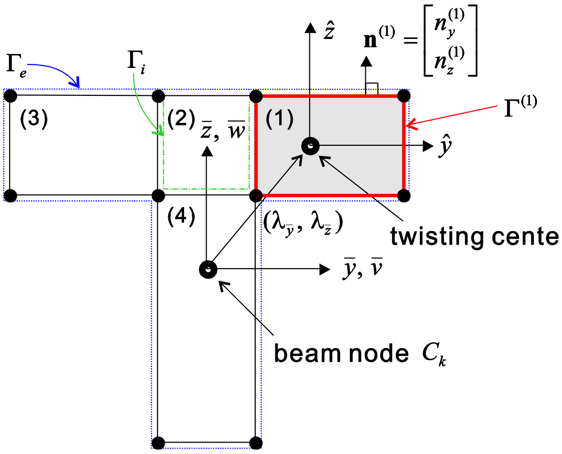

Fig. 2 A discretized composite cross-section using 4-node cross-sectional elements and its twisting center ($\lambda_{\bar{y}}, \lambda_{\bar{z}}$) in the cross-sectional Cartesian coordinate system

$$\text{with} \quad \overline{\mathbf{C}}^{(m)} = \begin{bmatrix} E^{(m)} & 0 & 0 \\ 0 & G^{(m)} & 0 \\ 0 & 0 & G^{(m)} \end{bmatrix} \tag{6}$$

where $E^{(m)}$ and $G^{(m)}$ represent the elastic and shear moduli, respectively, of sub-beam m. Note that this subdivision process facilitates the modeling of various material compositions.

For elastoplastic analysis of composite metallic beams, the 3D von Mises plasticity model with the associated flow rule and linear isotropic hardening in Refs. (Lee and McClure 2006, Neto *et al.* 2008, Kim *et al.* 2009) is employed. The constitutive equations are derived from a beam state projected onto the von Mises model. The conventional return mapping algorithm is adopted to solve the constitutive equations implicitly at each integration point. In practice, a higher-order Gauss integration scheme is required to obtain an accurate solution for elastoplastic analysis.

3. Warping functions for composite cross-sections

In this section, we propose a method to calculate the warping function for beams with an arbitrary composite cross-section. The warping function and the corresponding twisting center are simultaneously calculated based on the extended St. Venant equations, which are rooted in the previously developed method (Yoon and Lee 2014).

First, let us consider a discretized cross-sectional domain denoted using $\Omega = \bigcup_{m=1}^{n} \Omega^{(m)}$ on the beam cross-section k and its boundary $\Gamma = \Gamma_e \cup \Gamma_i$, where $\Omega^{(m)}$ is the domain corresponding to the cross-sectional element m, Γ_e is the external boundary, and Γ_i is the internal boundary, as shown in Fig. 2. The cross-sectional domain $\Omega^{(m)}$ has the elastic modulus $E^{(m)}$ and the shear modulus $G^{(m)}$.

It is important to note that we consider two parallel cross-sectional Cartesian coordinate systems defined in different origins: C_k (beam node) and $\hat{C}_k$ (twisting center).

In the cross-sectional domain m, the displacement field under pure twisting can be written as

$$\bar{u}^{(m)} = \alpha\, f_k^{(m)}, \quad \bar{v}^{(m)} = -\hat{z}^{(m)}\theta_x$$
$$\text{and} \quad \bar{w}^{(m)} = \hat{y}^{(m)}\theta_x \quad \text{in} \quad \Omega^{(m)} \tag{7}$$

where $\bar{u}$, $\bar{v}$ and $\bar{w}$ are the displacements in the $\bar{x}$ (longitudinal), $\bar{y}$ and $\bar{z}$ directions, respectively, $\alpha = \partial\theta_{\bar{x}}/\partial\bar{x}$, $f_k^{(m)}$ is the warping function, and $\hat{y}^{(m)}$ and $\hat{z}^{(m)}$ are the coordinates in the cross-sectional Cartesian coordinate system defined at the twisting center $\hat{C}_k$. This displacement field results in the following transverse shear stresses

$$\tau_{\bar{x}\bar{y}}^{(m)} = G^{(m)}\alpha\left(\frac{\partial f_k^{(m)}}{\partial\hat{y}} - \hat{z}^{(m)}\right)$$
$$\text{and} \quad \tau_{\bar{x}\bar{z}}^{(m)} = G^{(m)}\alpha\left(\frac{\partial f_k^{(m)}}{\partial\hat{z}} + \hat{y}^{(m)}\right) \quad \text{in} \quad \Omega^{(m)} \tag{8}$$

while other stress components are zero.

Substitution of Eq. (8) into the local equilibrium equations yields

$$G^{(m)}\left(\frac{\partial^2 f_k^{(m)}}{\partial\hat{y}^2} + \frac{\partial^2 f_k^{(m)}}{\partial\hat{z}^2}\right) = 0 \quad \text{in} \quad \Omega^{(m)} \tag{9}$$

Considering the transverse shear stress vector $\boldsymbol{\tau}^{(m)} = \left[\tau_{\bar{x}\bar{y}}^{(m)} \quad \tau_{\bar{x}\bar{z}}^{(m)}\right]^T$, the following boundary conditions should be satisfied for the cross-sectional domain m

$$\boldsymbol{\tau}^{(m)} \cdot \mathbf{n}^{(m)} = 0 \quad \text{on} \quad \Gamma_e \tag{10a}$$

$$\boldsymbol{\tau}^{(m)} \cdot \mathbf{n}^{(m)} + \boldsymbol{\tau}^{(m')} \cdot \mathbf{n}^{(m')} = 0 \quad \text{on} \quad \Gamma_i \tag{10b}$$

where $\mathbf{n}^{(m)}$ is the vector normal to the boundary Γ and m' denotes the adjacent domains, as shown in Fig. 2.

Combining Eq. (8) and Eq. (10) leads to the following equations

$$G^{(m)}\frac{\partial f_k^{(m)}}{\partial\mathbf{n}^{(m)}} = G^{(m)}\left(n_{\bar{y}}^{(m)}\hat{z}^{(m)} - n_{\bar{z}}^{(m)}\hat{y}^{(m)}\right) \quad \text{on} \quad \Gamma_e \tag{11a}$$

$$G^{(m)}\frac{\partial f_k^{(m)}}{\partial\mathbf{n}^{(m)}} + G^{(m')}\frac{\partial f_k^{(m')}}{\partial\mathbf{n}^{(m')}}$$
$$= G^{(m)}\left(n_{\bar{y}}^{(m)}\hat{z}^{(m)} - n_{\bar{z}}^{(m)}\hat{y}^{(m)}\right) \tag{11b}$$
$$+ G^{(m')}\left(n_{\bar{y}}^{(m')}\hat{z}^{(m)} - n_{\bar{z}}^{(m')}\hat{y}^{(m)}\right) \quad \text{on} \quad \Gamma_i$$

Considering the boundary of the cross-sectional domain m ($\Gamma^{(m)}$), both Eqs. 11(a) and (b) can be rewritten as

$$G^{(m)}\frac{\partial f_k^{(m)}}{\partial\mathbf{n}^{(m)}} = G^{(m)}\left(n_{\bar{y}}^{(m)}\hat{z}^{(m)} - n_{\bar{z}}^{(m)}\hat{y}^{(m)}\right) \quad \text{on} \quad \Gamma^{(m)} \tag{12}$$

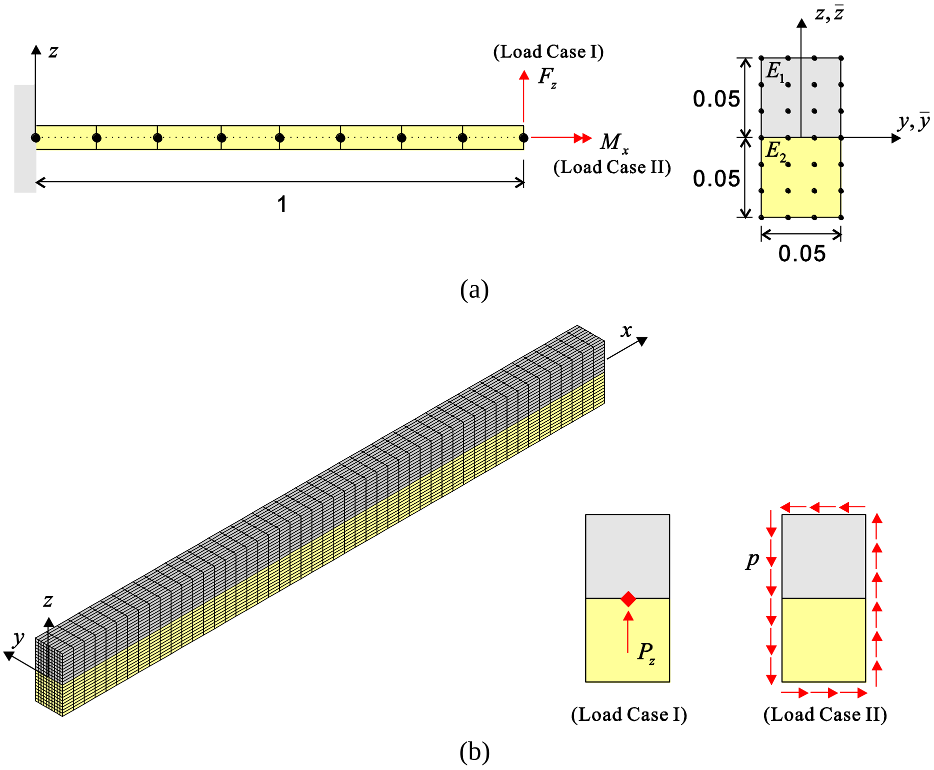

Fig. 3 Rectangular composite beam problem (unit: m): (a) longitudinal and cross-sectional meshes used in the beam model (8 beam elements, 63 DOFs) and (b) solid element model (10,000 solid elements, 11,781 DOFs) used

The variational formulation can be easily derived from Eq. (9) with the variation of the warping function $\delta f_k^{(m)}$

$$\sum_{m=1}^{n}\left[\int_{\Omega^{(m)}} G^{(m)}\left(\frac{\partial f_k^{(m)}}{\partial \hat{y}}\frac{\partial \delta f_k^{(m)}}{\partial \hat{y}}+\frac{\partial f_k^{(m)}}{\partial \hat{z}}\frac{\partial \delta f_k^{(m)}}{\partial \hat{z}}\right)d\Omega^{(m)}\right] = \sum_{m=1}^{n}\left[\int_{\Gamma^{(m)}} G^{(m)}\frac{\partial f_k^{(m)}}{\partial \mathbf{n}^{(m)}}\delta f^{(m)}\, d\Gamma^{(m)}\right] \tag{13}$$

Substituting the boundary condition Eq. (12) into Eq. (13), the finite element formulation for the extended St. Venant equations is obtained as

$$\sum_{m=1}^{n}\left[\int_{\Omega^{(m)}} G^{(m)}\left(\frac{\partial f_k^{(m)}}{\partial \hat{y}}\frac{\partial \delta f_k^{(m)}}{\partial \hat{y}}+\frac{\partial f_k^{(m)}}{\partial \hat{z}}\frac{\partial \delta f_k^{(m)}}{\partial \hat{z}}\right)d\Omega^{(m)}\right] = \sum_{m=1}^{n}\left[\int_{\Gamma^{(m)}} G^{(m)}\left(n_{\bar{y}}^{(m)}\hat{z}^{(m)} - n_{\bar{z}}^{(m)}\hat{y}^{(m)}\right)\delta f^{(m)}\, d\Gamma^{(m)}\right] \tag{14}$$

Using the relation between the two cross-sectional Cartesian coordinate systems denoted as $(\bar{y}, \bar{z})$ and $(\hat{y}, \hat{z})$, $\hat{y} = \bar{y} - \lambda_{\bar{y}}$ and $\hat{z} = \bar{z} - \lambda_{\bar{z}}$, in Eq. (14), we obtain

$$\begin{aligned}&\sum_{m=1}^{n}\left[\int_{\Omega^{(m)}} G^{(m)}\left(\frac{\partial f_k^{(m)}}{\partial \bar{y}}\frac{\partial \delta f_k^{(m)}}{\partial \bar{y}}+\frac{\partial f_k^{(m)}}{\partial \bar{z}}\frac{\partial \delta f_k^{(m)}}{\partial \bar{z}}\right)d\Omega^{(m)}\right] \\ &+ \sum_{m=1}^{n}\left[\int_{\Gamma^{(m)}} G^{(m)}\lambda_{\bar{z}} n_{\bar{y}}^{(m)}\delta f^{(m)}\, d\Gamma^{(m)}\right] - \sum_{m=1}^{n}\left[\int_{\Gamma^{(m)}} G^{(m)}\lambda_{\bar{y}} n_{\bar{z}}^{(m)}\delta f^{(m)}\, d\Gamma^{(m)}\right] \\ &= \sum_{m=1}^{n}\left[\int_{\Gamma^{(m)}} G^{(m)}\left(n_{\bar{y}}^{(m)}\bar{z}^{(m)} - n_{\bar{z}}^{(m)}\bar{y}^{(m)}\right)\delta f^{(m)}\, d\Gamma^{(m)}\right]\end{aligned} \tag{15}$$

Zero bending moment conditions ($M_{\hat{z}} = M_{\hat{y}} = 0$) for beams under pure twisting give

$$\sum_{m=1}^{n}\left[\int_{\Omega^{(m)}} E^{(m)} f_k^{(m)} (\bar{y} - \bar{y}_{ave})\, d\Omega^{(m)}\right] = 0 \tag{16a}$$

$$\sum_{m=1}^{n}\left[\int_{\Omega^{(m)}} E^{(m)} f_k^{(m)} (\bar{z} - \bar{z}_{ave})\, d\Omega^{(m)}\right] = 0 \tag{16b}$$

with the location of the cross-sectional centroid $(\bar{y}_{ave}, \bar{z}_{ave})$,

$$\bar{y}_{ave} = \frac{\sum_{m=1}^{n}\int_{\Omega^{(m)}} \bar{y}\, d\Omega^{(m)}}{\sum_{m=1}^{n}\int_{\Omega^{(m)}} d\Omega^{(m)}} \quad \text{and} \quad \bar{z}_{ave} = \frac{\sum_{m=1}^{n}\int_{\Omega^{(m)}} \bar{z}\, d\Omega^{(m)}}{\sum_{m=1}^{n}\int_{\Omega^{(m)}} d\Omega^{(m)}} \tag{17}$$

Eqs. (15) and (16) are discretized by interpolating the warping function $f_k^{(m)}$ and its variation $\delta f_k^{(m)}$ using the same interpolation as in Eq. (2) represented by

$$f_k^{(m)} = \mathbf{H}^{(m)}\mathbf{F}^{(m)} = \mathbf{H}^{(m)}\mathbf{L}^{(m)}\mathbf{F} \tag{18}$$

$$\text{with} \quad \mathbf{H}^{(m)} = \left[h_1(s,t) \quad h_2(s,t) \quad \cdots \quad h_p(s,t)\right] \tag{19a}$$

$$\mathbf{F}^{(m)} = \left[f_k^{1(m)} \quad f_k^{2(m)} \quad \cdots \quad f_k^{p(m)} \right]^T \tag{19b}$$

$$\mathbf{F} = \left[f_k^{1} \quad f_k^{2} \quad \cdots \quad f_k^{l} \right]^T \tag{19c}$$

in which $\mathbf{L}^{(m)}$ is the standard assemblage Boolean matrix for the cross-sectional element m, $\mathbf{F}^{(m)}$ is the elemental warping DOFs vector, $\mathbf{F}$ is the entire warping DOFs vector, and l denotes the number of cross-sectional nodes.

Finally, the following equations in matrix form are obtained

$$\begin{bmatrix} \mathbf{K} & \mathbf{N}_{\bar{y}} & \mathbf{N}_{\bar{z}} \\ \mathbf{H}_{\bar{y}} & \mathbf{0} & \mathbf{0} \\ \mathbf{H}_{\bar{z}} & \mathbf{0} & \mathbf{0} \end{bmatrix} \begin{bmatrix} \mathbf{F} \\ \lambda_{\bar{z}} \\ \lambda_{\bar{y}} \end{bmatrix} = \begin{bmatrix} \mathbf{B} \\ 0 \\ 0 \end{bmatrix} \tag{20}$$

in which

$$\mathbf{K} = \sum_{m=1}^{n} \int_{\Omega^{(m)}} G^{(m)} \mathbf{L}^{(m)T} \left(\frac{\partial \mathbf{H}^{(m)T}}{\partial \bar{y}} \frac{\partial \mathbf{H}^{(m)}}{\partial \bar{y}} + \frac{\partial \mathbf{H}^{(m)T}}{\partial \bar{z}} \frac{\partial \mathbf{H}^{(m)}}{\partial \bar{z}} \right) \mathbf{L}^{(m)} d\Omega^{(m)} \tag{21a}$$

$$\mathbf{N}_{\bar{y}} = \sum_{m=1}^{n} \int_{\Omega^{(m)}} G^{(m)} n_{\bar{y}}^{(m)} \mathbf{L}^{(m)T} \mathbf{H}^{(m)T} d\Omega^{(m)} \tag{21b}$$

$$\mathbf{N}_{\bar{z}} = \sum_{m=1}^{n} \int_{\Omega^{(m)}} G^{(m)} n_{\bar{z}}^{(m)} \mathbf{L}^{(m)T} \mathbf{H}^{(m)T} d\Omega^{(m)} \tag{21c}$$

$$\mathbf{B} = \sum_{m=1}^{n} \int_{\Gamma^{(m)}} G^{(m)} \left(n_{\bar{y}}^{(m)} \bar{z}^{(m)} - n_{\bar{z}}^{(m)} \bar{y}^{(m)} \right) \mathbf{L}^{(m)T} \mathbf{H}^{(m)T} d\Gamma^{(m)} \tag{21d}$$

$$\mathbf{H}_{\bar{y}} = \sum_{m=1}^{n} \int_{\Omega^{(m)}} E^{(m)} \left(\bar{y} - \bar{y}_{ave} \right) \mathbf{H}^{(m)} \mathbf{L}^{(m)} d\Omega^{(m)} \tag{21e}$$

$$\mathbf{H}_{\bar{z}} = \sum_{m=1}^{n} \int_{\Omega^{(m)}} E^{(m)} \left(\bar{z} - \bar{z}_{ave} \right) \mathbf{H}^{(m)} \mathbf{L}^{(m)} d\Omega^{(m)} \tag{21f}$$

We can calculate the warping function as well as the corresponding twisting center at the same time by solving Eq. (20).

4. Numerical examples

Here we demonstrate the performance of the proposed beam element through several representative numerical examples. The standard full Newton-Raphson iterative scheme is employed for the solution of nonlinear problems. Solutions obtained using the proposed beam element are compared with reference solutions obtained using finely meshed 3D solid finite element models in ADINA (ADINA R&D 2013).

4.1 Rectangular composite beam problem

We consider a straight cantilever beam with a length of L=1 m and a rectangular composite cross-section, as illustrated in Fig. 3. The beam is modeled using eight continuum mechanics based beam elements whose cross-section is discretized using two 16-node cubic cross-sectional elements. Various Young's modulus ratios (E_2/E_1) are considered with fixed $E_1=1.0\times10^{11}$ N/m^2 and Poisson's ratio v=0. The fully clamped boundary condition applied is $u=v=w=\theta_x=\theta_y=\theta_z=\alpha=0$ at x=0 m. Loading conditions are

- Load Case I: The shear force F_z=100 kN is applied at the free tip (x=1 m).
- Load Case II: The torsion M_x=40 kN·m is applied at the free tip (x=1 m).

Reference solutions are obtained using ten thousand 8-node solid elements in the finite element model shown in Fig. 3(b). All degrees of freedom are fixed at x=0 m. A point load P_z=100 kN is applied at x=1 m for Load Case I while a distributed line load p=2000 kN/m around the cross-section is applied at x=1 m for Load Case II.

Table 1 presents the deflection under Load Case I and

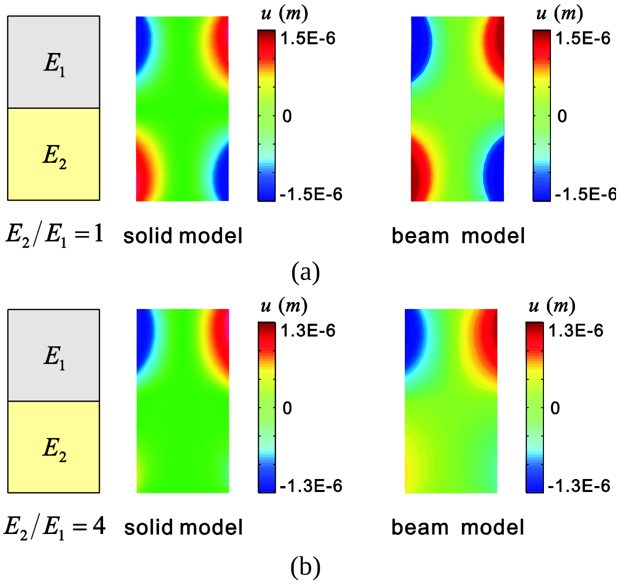

Fig. 4 Longitudinal displacements in the cross-section for the rectangular composite cross-section beam problem: (a) E_2/E_1=1 and (b) E_2/E_1=4

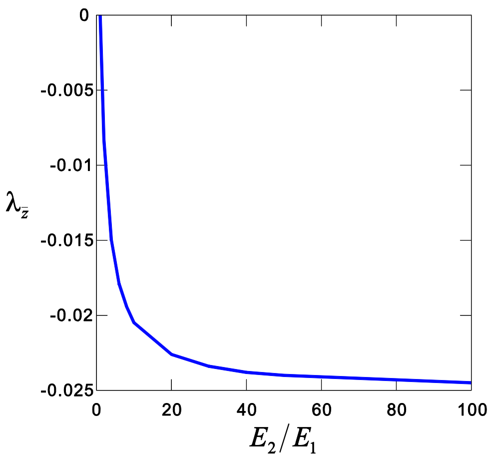

Fig. 5 Position $\lambda_{\bar{z}}$ of the twisting center according to Young's modulus ratio E_2/E_1 in the rectangular composite cross-section problem ($\lambda_{\bar{y}}=0$)

Table 1 Numerical results in the rectangular composite beam problem.

$\frac{E_2}{E_1}$	Load Case I, Deflection (m)			Load Case II, Twisting angle (rad)		
	Solid model	Proposed beam model	Difference (%)	Solid model	Proposed beam model	Difference (%)
1.0	0.08059	0.08009	0.6204	0.27047	0.27672	2.3107
2.0	0.05860	0.05822	0.6485	0.18840	0.19283	2.3514
3.0	0.04956	0.04924	0.6457	0.14970	0.15330	2.4048
4.0	0.04412	0.04382	0.6800	0.12568	0.12876	2.4507
5.0	0.04025	0.03998	0.6708	0.10886	0.11157	2.4894

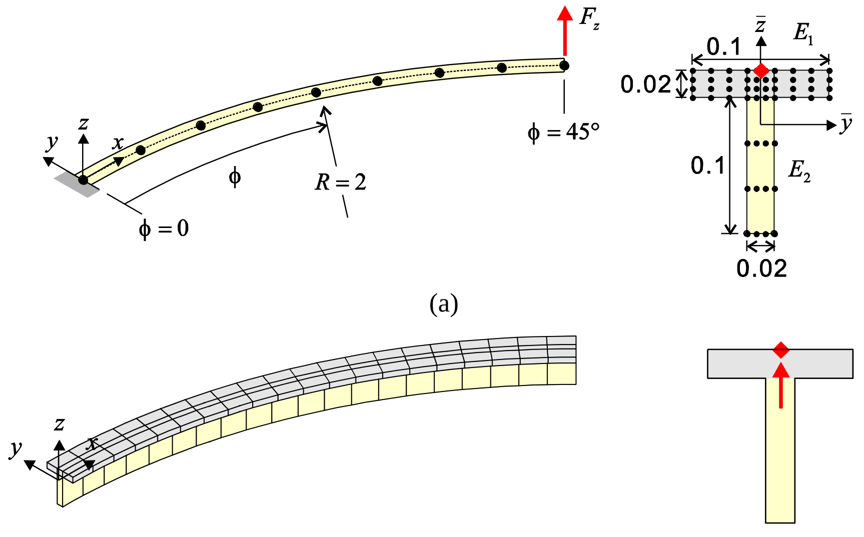

Fig. 6 45-degree bend beam problem (unit: m): (a) longitudinal and cross-sectional meshes used in the beam model (8 beam elements, 63 DOFs) and (b) solid element model (80 solid elements, 3,321 DOFs) used

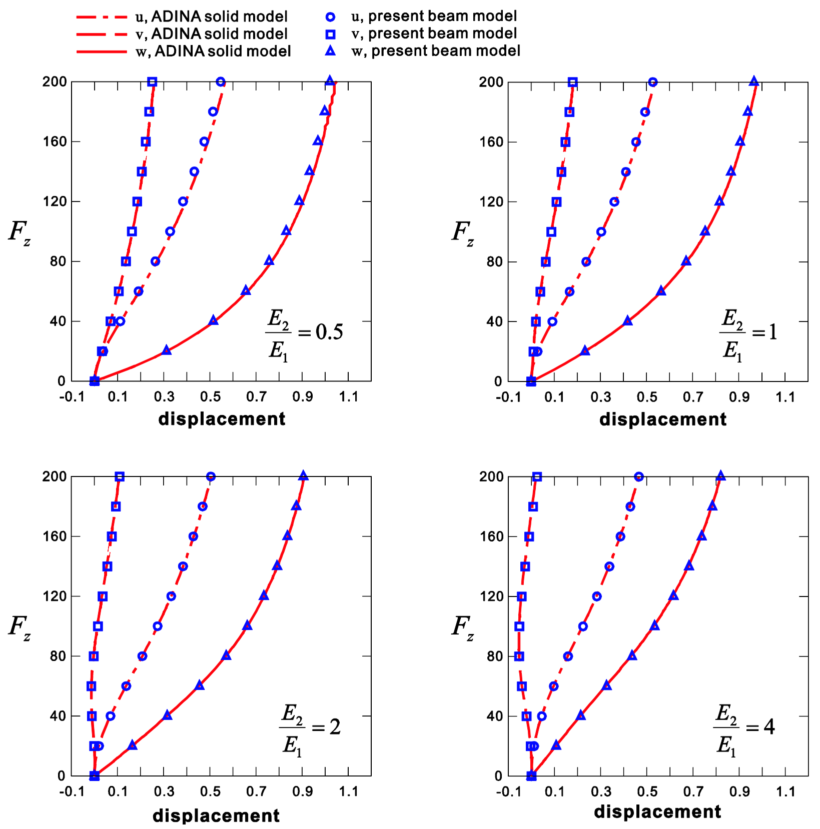

Fig. 7 Load-displacement curves according to various composition ratios in the 45-degree bend beam problem

Table 2 Shear stresses at point A and torsional constants (I_t) in the square cross-section with circular inclusion

$\frac{E_2}{E_1}$	τ_{xy} (kPa)				I_t (m^4)		
	Sapountzakis (τ_{xy}^{p})		Proposed beam model		Sapountzakis	Proposed beam model	Difference (%)
	Matrix	Inclusion	Matrix	Inclusion			
0.0	21.8998	0	24.149	0	0.1344	0.1331	0.9673
1.0	19.3489	19.3489	21.627	22.660	0.1406	0.1392	0.9957
4.0	16.2734	65.0815	17.897	75.020	0.1590	0.1580	0.6289
6.0	14.9615	89.7487	16.292	102.45	0.1712	0.1706	0.3505
8.0	13.8862	111.0617	15.005	125.81	0.1835	0.1832	0.1635
10.0	12.9715	129.6811	13.931	146.01	0.1958	0.1959	0.0511

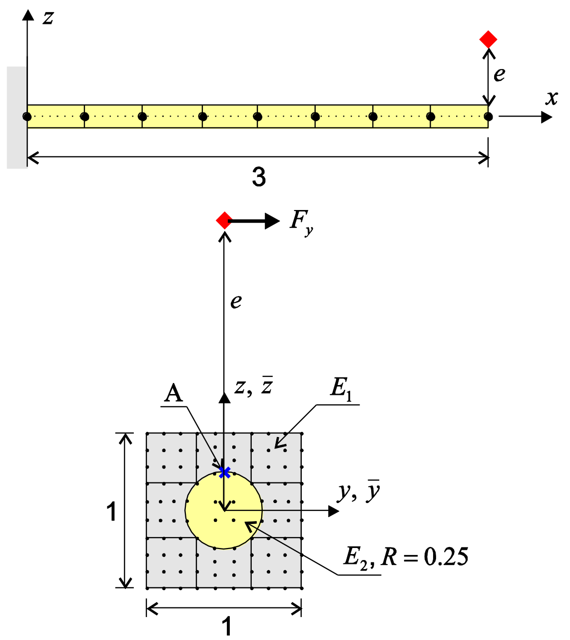

Fig. 8 Beam problem of the square cross-section with circular inclusion and its longitudinal and cross-sectional meshes (unit: *m*)

the twist angle under Load Case II at the free tip (x=1 m) for various Young's modulus ratios. The results obtained using the beam element model (in total 63 DOFs) with the proposed composite warping displacement agree well with the reference solutions obtained using the solid element model (in total 11,781 DOFs). Fig. 4 shows the distributions of the displacement in the x-direction on the cross-sectional plane at x=0.5 m, illustrating the excellent predictive capability of the composite warping displacement model proposed in this study. Fig. 5 displays the $\bar{z}$-directional position of the twisting center ($\lambda_{\bar{z}}$) calculated according to Young's modulus ratio E_2/E_1. The expected shifting of the twisting center is well observed.

4.2 45-degree bend beam problem

A 45-degree circular cantilever beam of radius R=2 m has a T-shaped cross-section, as shown in Fig. 6(a). The beam is modeled by eight continuum mechanics based beam elements. The beam cross-section is discretized using four 16-node cubic cross-sectional elements. We consider various Young's modulus ratios (E_2/E_1) with fixed E_1=5.0×10^{10} N/m^2 and Poisson's ratio $\nu = 0.3$. At ϕ=0°, the beam is fully clamped: u=v=w=θ_x=θ_y=θ_z=α=0. The z-directional load F_z is applied at free tip (ϕ=45°).

Reference solutions are obtained using eighty 27-node solid elements in the finite element model shown in Fig. 6(b). In the solid model, all degrees of freedom are fixed at ϕ=0°, and a point load F_z is applied at ϕ=45°.

The accurate solution of this curved beam problem is hard to obtain without properly considering the flexure–torsion coupling effect. Fig. 7 displays the load-displacement curves for various material composition ratios E_2/E_1. The proposed beam element model provides good agreement with the reference solutions. It is interesting to note that the direction of the displacement v varies depending on the material composition ratios due to bending-twisting coupling effects.

4.3 Square cross-section with circular inclusion

We consider the benchmark problem proposed by Sapountzakis and Mokos (Sapountzakis and Mokos 2003) under small displacement assumption. As shown in Fig. 8, a straight cantilever beam of L=3 m is considered that has a

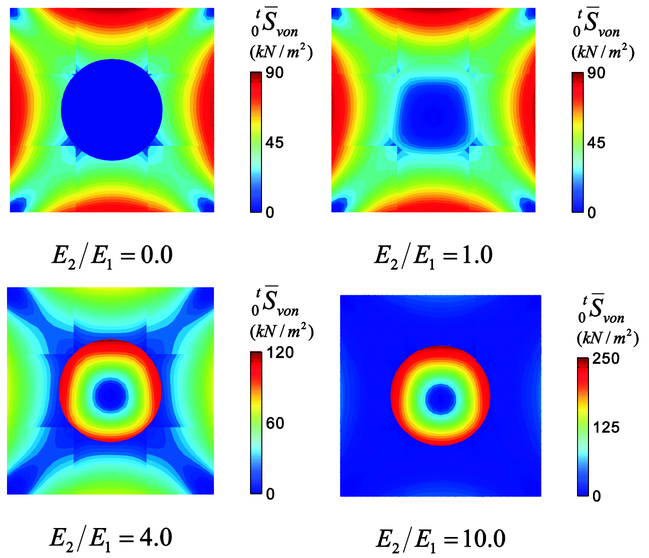

Fig. 9 Distributions of the von Mises stress in the square cross-section with circular inclusion

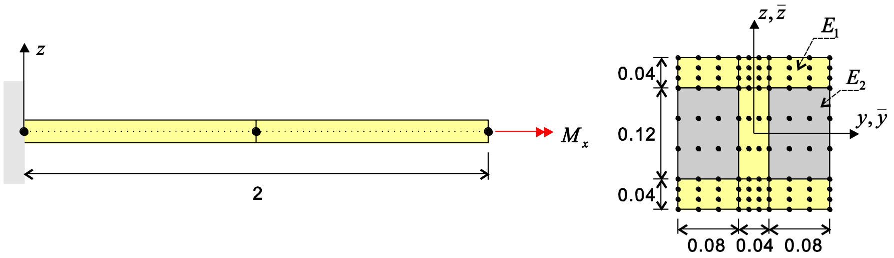

(a)

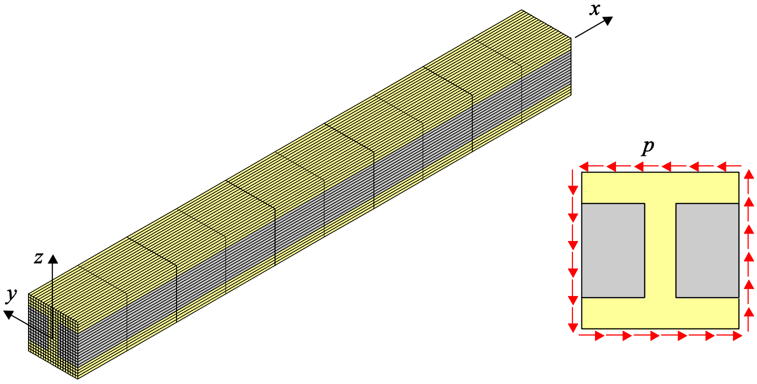

(b)

Fig. 10 Reinforced wide-flange beam problem (unit: *m*): (a) longitudinal and cross-sectional meshes used in the beam model (2 beam elements, 21 DOFs) and (b) solid element model (4,000 solid elements, 35,301 DOFs) used

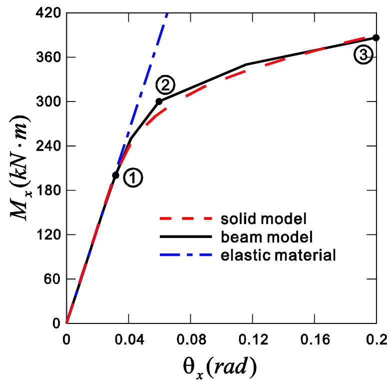

(a)

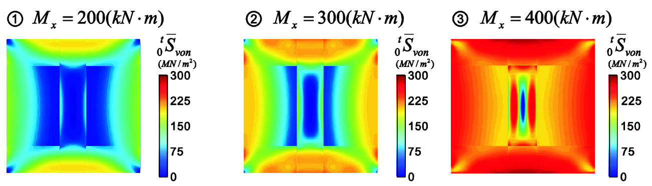

(b)

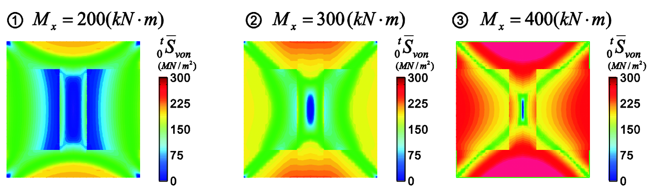

(c)

Fig. 11 Numerical results for the reinforced wide-flange beam problem: (a) load-displacement curves, (b) distributions of the von Mises stress obtained using the proposed beam element model, and (c) distributions of the von Mises stress obtained using the solid element model

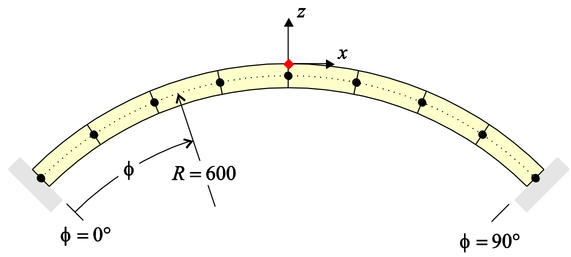

(a)

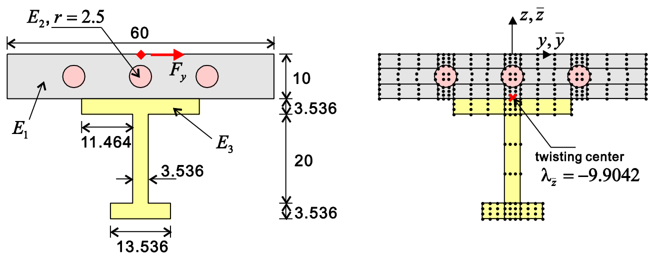

(b)

Fig. 12 90-degree circular arch problem (unit: cm): (a) longitudinal meshes used in the beam model (8 beam elements) and (b) cross-sectional meshes used (63 DOFs)

square cross-section with circular inclusion. The beam is modeled using eight 2-node continuum mechanics based beam elements. The cross-section is discretized using nine 16-node cubic cross-sectional elements. The boundary condition $u=v=w=\theta_x=\theta_y=\theta_z=\alpha=0$ is applied at x=0 m. The y-directional concentrated load F_y=2 kN is applied at x=3 m with eccentricity e=5 m. Various Young's modulus ratio (E_2/E_1) are tested with fixed $E_1=3.0\times10^{10}$ N/m^2 and Poisson's ratio ν=0.2.

Table 2 lists the shear stresses τ_{xy} at point A and the

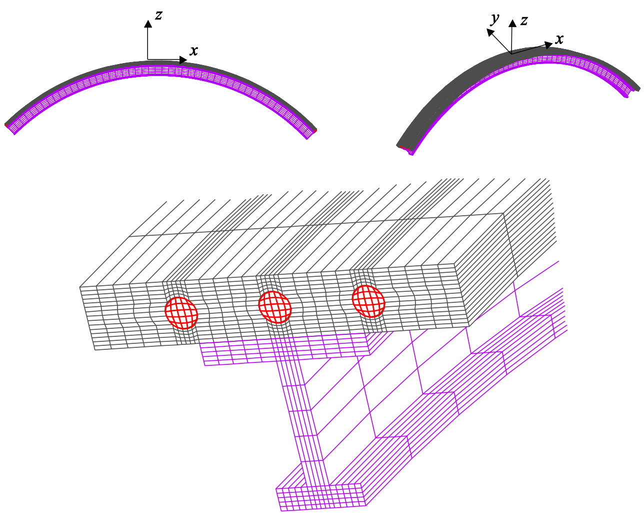

Fig. 13 Solid element model for the 90-degree circular arch problem (35,000 solid elements, 118,728 DOFs)

torsional constants I_t (=$M_xL/G_1\theta_x$) for various Young's modulus ratios. The results predicted by the proposed beam element are in good agreement with the reference solutions obtained by Sapountzakis and Mokos (Sapountzakis and Mokos 2003). Note that, based on Jourawski's theory, they considered both primary and secondary warping functions but the shear stresses obtained by Sapountzakis in Table 2 include only the primary shear stress term corresponding to the primary warping function. Fig. 9 illustrates the distributions of the von Mises stress on the cross-section at x=3 m obtained using the proposed beam element. Variations in the stress distribution with respect to the ratio of Young's modulus are well captured.

4.4 Reinforced wide-flange beam problem

We consider a straight cantilever beam with a length of L=2 m with a reinforced wide-flange cross-section, as shown in Fig. 10(a), consisting of two different elasto-plastic materials:

- Material 1 (yellow colored): Young's modulus E_1=2.0×10^{11} N/m^2, Poisson's ratio v_1=0, hardening modulus H_1=0.1, and yield stress Y_1=2.0×10^8 N/m^2,
- Material 2 (gray colored): Young's modulus E_1=0.7×10^{11} N/m^2, Poisson's ratio v_2=0, hardening modulus H_2=0.1, and yield stress Y_2=2.0×10^8 N/m^2.

The beam is modeled using two beam elements whose cross-section is discretized using nine 16-node cubic cross-sectional elements. The fully clamped boundary condition is applied at x=0 m and the twisting moment M_x is applied at the free tip (x=2 m).

Reference solutions are obtained using four thousand 27-node solid elements in the finite element model illustrated in Fig. 10(b). All degrees of freedom are fixed at x=0 m, and the line load p=12.5 M_x is distributed around the cross-section at the free tip (x=2 m).

Fig. 11(a) displays the load-displacement curves calculated using 16 incremental load steps. The results obtained using the beam element model (in total 21 DOFs) match well with the reference solutions computed using the solid element model (in total 35,301 DOFs).

Figs. 11(b) and (c) illustrate the distributions of the von

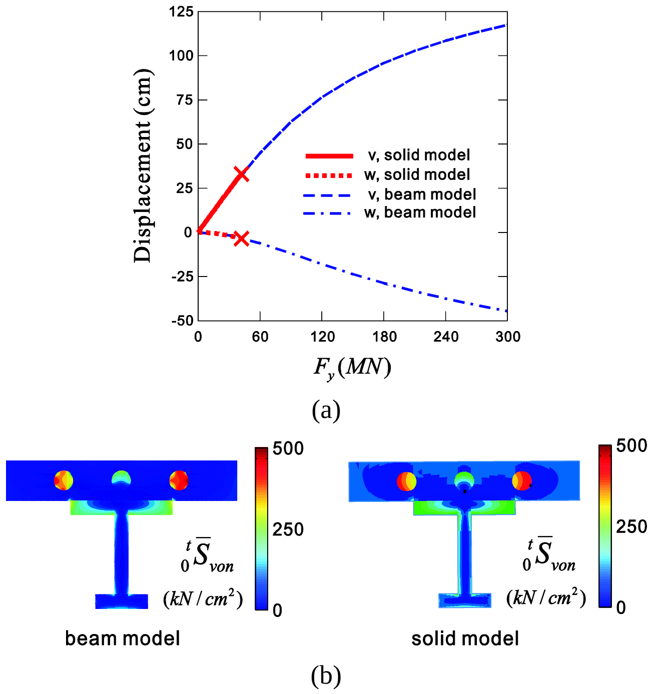

Fig. 14 Numerical results for the 90-degree circular arch problem: (a) load-displacement curves, (b) distributions of the von Mises stress obtained using the proposed beam and solid element models

Mises stress on the cross-section at x=1 m in the beam and solid element models, respectively, where we can observe that the propagation of the yield region is well predicted using the beam element model.

4.5 90-degree circular arch problem

We consider a 90-degree circular arch of radius R=600 cm with a composite cross-section, as shown in Fig. 12. The beam is modeled using eight 2-node continuum mechanics based beam elements. The cross-section is discretized using twenty-eight 16-node cubic cross-sectional elements. The boundary condition u=v=w=θ_x=θ_y=θ_z=α=0 is applied at ϕ=0° and ϕ=90°, while the y-directional concentrated load F_y is applied at ϕ=45° (marked by a red dot). The cross-section consists of three different materials.

- Material 1: Young's modulus E_1=3.0×10^7 N/m^2, Poisson's ratio v_1=0.
- Material 2: Young's modulus E_2=3.0×10^8 N/m^2, Poisson's ratio v_2=0.
- Material 3: Young's modulus E_3=2.0×10^8 N/m^2, Poisson's ratio v_3=0.

To obtain the reference solutions, thirty five thousand 8-node solid elements are used in the solid element model illustrated in Fig. 13. All degrees of freedom are fixed at ϕ=0° and ϕ=90°, while a concentrated load F_y is applied at ϕ=45°.

Fig. 14(a) compares the load-displacement curves obtained using the solid and beam element models. Solutions up to F_y=300 MN can be easily obtained in ten load steps when we use the proposed beam element. However, when we use the solid element model, the solution procedure is terminated quite early even though five hundred load steps with line search algorithms are used. Fig. 14(b) shows the distributions of the von Mises stress on the cross-section at ϕ=22.5° in the beam and solid element models when F_y=300 MN is applied. Note that, in order to obtain appropriate responses in this beam problem, coupled behaviors among stretching, bending, shearing, twisting, and warping must be properly modeled.

5. Conclusions

In this paper, we presented a nonlinear finite element formulation for arbitrary composite cross-section beams. The element was developed within continuum mechanics based framework so that it can handle the complexity in geometry and material properties of beam cross-sections with ease. The warping function and the corresponding twisting center were computed by solving the extended St. Venant equations numerically on a discretized cross-section. The excellent performance of the proposed beam element in geometric and/or material nonlinear problems was demonstrated through various representative numerical examples.

While we applied only the proposed element to nonlinear static problems in this study, it can be easily extended for analysis of nonlinear dynamic problems where the inertia effect of the cross-section needs to be properly modeled as well, which is worthwhile to investigate.

Acknowledgments

This work was supported by the Basic Science Research Program through the National Research Foundation of Korea (NRF) funded by the Ministry of Science, ICT & Future Planning (NRF-2014R1A1A1A05007219) and also by the Convergence Research Program for Sports Scientification through the National Research Foundation of Korea (NRF) funded by the Ministry of Science, ICT & Future Planning (NRF-2014M3C1B1033983).

References

ADINA R&D (2013), *ADINA Theory and Modeling Guide*, Watertown, MA: ADINA R&D.

Bathe, K.J. (2014), *Finite Element Procedures*, 2nd Edition, Watertown, MA.

Cardoso, J.E.B., Benedito, N.M.B. and Valido, A.J.J. (2009), "Finite element analysis of thin-walled composite laminated beams with geometrically nonlinear behavior including warping deformation", *Thin Wall. Struct*., **47**, 1363-1372.

Cortinez, V.H. and Piovan, M.T. (2006), "Stability of composite thin-walled beams with shear deformability", *Comput. Struct*., **84**, 978-990.

Fatmi, R.E. and Ghazouani, N. (2011), "Higher order composite beam theory built on Saint-Venant's solution. Part-I: Theoretical developments", *Compos. Struct*., **93**, 557-566.

Genoese, A., Genoese, A., Bilotta, A. and Garcea, G. (2014), "A composite beam model including variable warping effects derived from a generalized Saint Venant solution", *Compos. Struct*., **110**, 140-151.

Hodges, D.H. (2006), *Nonlinear Composite Beam Theory*, American Institute of Aeronautics and Astronautics, Reston, Virginia.

Høgsberg, J. and Krenk, S. (2014), "Analysis of moderately thin-walled beam cross-sections by cubic isoparametric elements", *Comput. Struct*., **134**, 88-101.

Horgan, C.O. Simmonds, J.G. (1994), "Saint Venant end effects in composite structures", *Compos. Engrg*., **4**, 279-286.

Ishaquddin, Md., Raveendranath, P. and Reddy, J.N. (2012), "Flexure and torsion locking phenomena in out-of-plane deformation of Timoshenko curved beam element", *Finite Elem. Anal. Des*., **51**, 22-30.

Kim, D.N., Montans F.J. and Bathe, K.J. (2009), "Insight into a model for large strain anisotropic elasto-plasticity", *Comput. Mech*., **44**, 2027-2041.

Lee, J. and Lee, S. (2004), "Flexural-torsional behavior of thin-walled composite beams", *Thin Wall. Struct*., **42**, 1293-1305.

Lee, P.S. and McClure, G. (2006), "A general 3D L-section beam finite element for elastoplastic large deformation analysis", *Comput. Struct*., **84**, 215-229.

Librescu, L. (2006), *Thin-walled Composite Beams*, Springer, Dordrecht.

Neto, E.A.S, Perić, D. and Owen, D.R.J. (2008), *Computational Method for Plasticity: Theory and Applications*, Wiley & Sons.

Rand, O. (1998), "Closed-form solutions for solid and thin-walled composite beams including a complete out-of-plane warping model", *Int. J. Solid. Struct*., **35**, 2775-2793.

Sapountzakis E.J. and Mokos V.G. (2003), "Warping shear stresses in nonuniform torsion of composite bars by BEM", *Comput. Meth. Appl. Mech. Eng*., **192**, 4337-4353.

Sapountzakis, E.J. and Tsipiras, V.J. (2010), "Non-linear elastic non-uniform torsion of bars of arbitrary cross-section by BEM", *Int. J. Nonlin. Mech*., **45**, 63-74.

Timoshenko, S.P. and Goodier, J.N. (1970), *Theory of Elasticity*, McGraw Hill.

Tsai, S.W. (1992), *Theory of Composites Design*, Think Composites.

Tsipiras V.J. and Sapountzakis E.J. (2012), "Secondary torsional moment deformation effect in inelastic nonuniform torsion of bars of doubly symmetric cross section by BEM", *Int. J. Nonlin. Mech*., **47**, 68-84.

Vlasov, V.Z. (1961), *Thin-walled Elastic Beams*, Israel Program for Scientific Translations, Jerusalem.

Yoon, K. and Lee, P.S. (2014), "Nonlinear performance of continuum mechanics based beam elements focusing on large twisting behaviors", *Comput. Meth. Appl. Mech. Eng*., **281**, 106-130.

Yoon, K. Lee, Y.G., Lee, P.S. (2012), "A continuum mechanics based beam finite element with warping displacements and its modeling capabilities", *Struct. Eng. Mech*., **43**, 411-437.

CC